PNAS
www.pnas.org

Supplementary Information for

The *Shh*/*Gli3* gene regulatory network precedes the origin of paired fins and reveals the deep homology between distal fins and digits.

Joaquín Letelier[a,b,1], Silvia Naranjo[a,1], Ismael Sospedra-Arrufat[a], Juan Ramón Martinez-Morales[a], Javier Lopez-Rios[a,2], Neil Shubin[c,2] and José Luis Gómez-Skarmeta[a].

[2]Corresponding authors: Javier Lopez-Rios, Neil Shubin
Email: jloprio@upo.es; nshubin@uchicago.edu

This PDF file includes:

Figures S1 to S7
Table S1

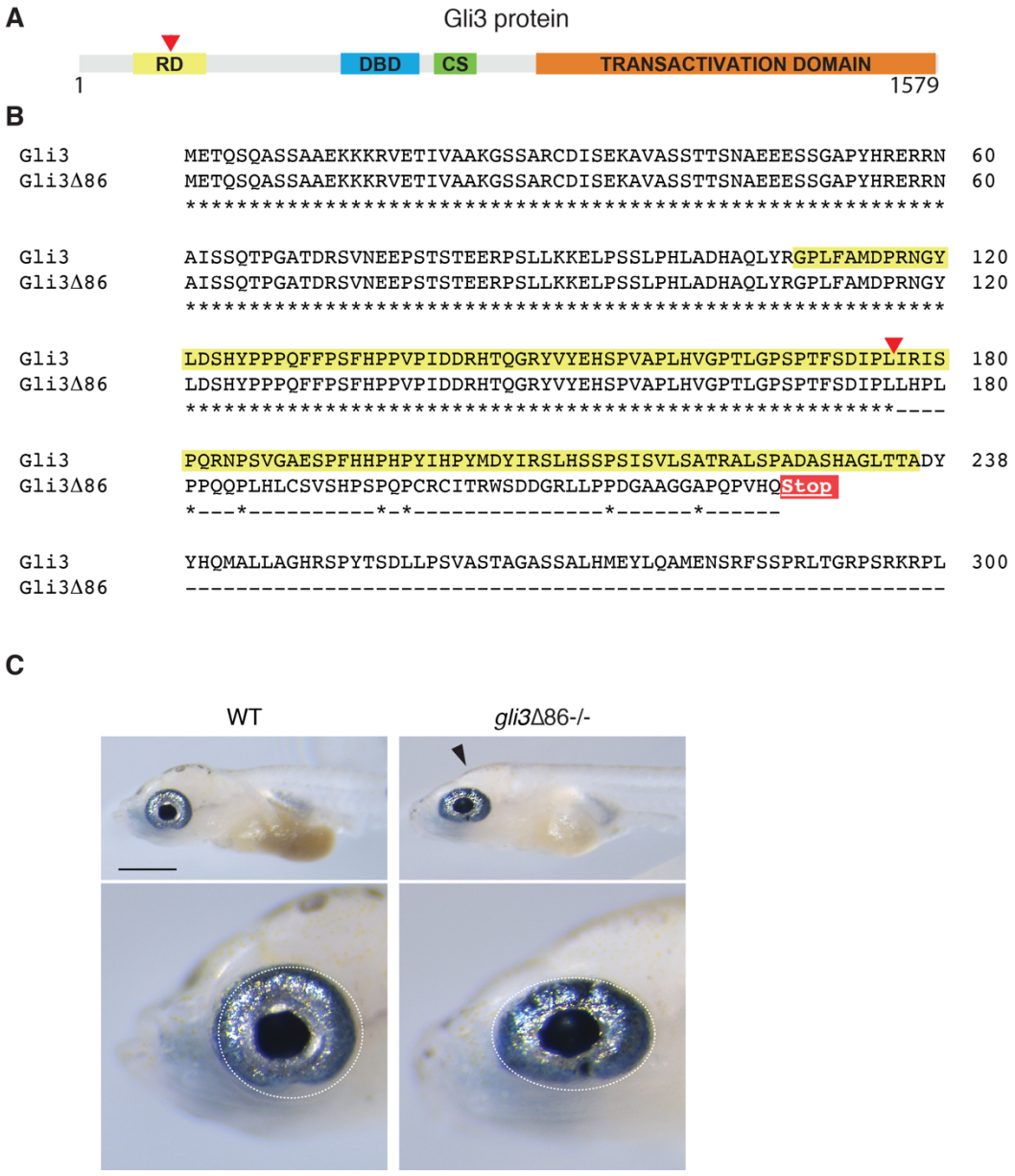

Fig. S1. The *gli3*Δ86 CRISPR/Cas9-induced mutation truncates the Gli3 protein at the level of the N-terminal repressor domain.

(A) Domain structure of the medaka Gli3 protein. RD: repressor domain (yellow), DBD: DNA binding domain (blue), CS: cleavage site (green) and transactivation domain (red). (B) The Δ86 mutation (red arrowhead) generates a frameshift change in the middle of the region encoding the Gli3 repressor domain (yellow amino acid sequence) that results in a premature STOP codon that truncates the predicted protein upstream of the DBD. (C) Malformations observed in *gli3*Δ*86* homozygous mutants at 3 weeks of age include abnormal head morphology (arrowhead) and oval-shaped eyes.

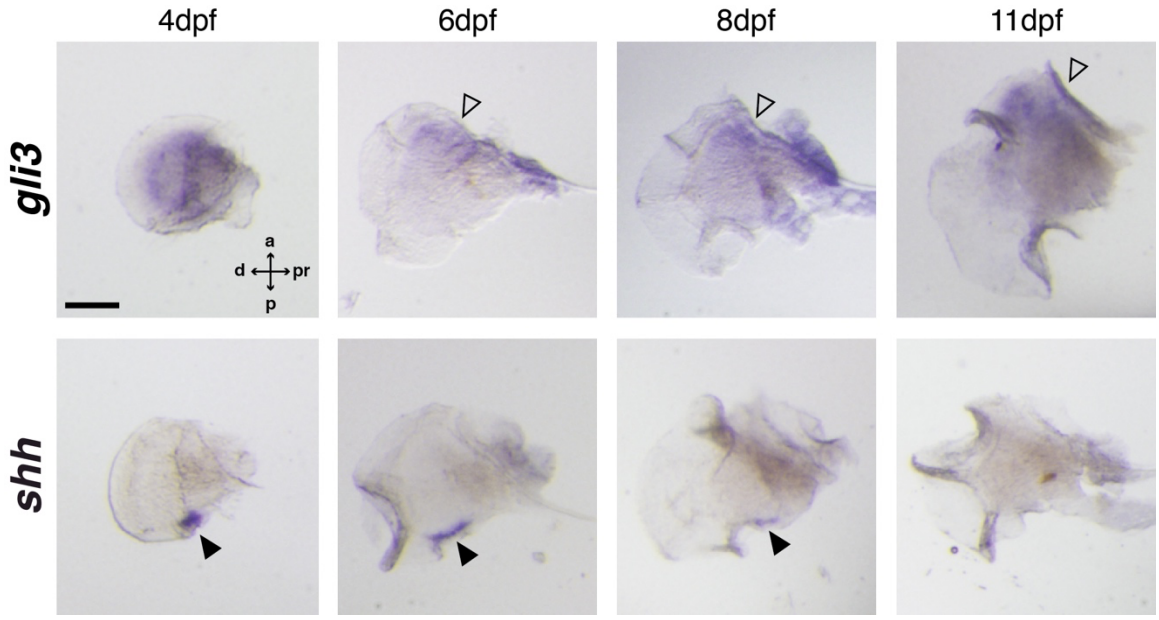

Fig. S2. Expression dynamics of *gli3* and *shh* in medaka pectoral fins.

Analysis of the distribution of *gli3* and *shh* transcripts in wild-type medaka pectoral fins at 4, 6, 8 and 11 days post-fertilization (dpf; n≥3 per probe and stage). *gli3* transcription is initially detected throughout the entire 4dpf endochondral disc, becoming more prominent in the anterior margin from 6 dpf onward (open arrowheads). Robust *shh* expression is detected in in the posterior mesenchyme (black arrowheads) at 4 and 6 dpf. *shh* expression is progressively extinguished at advanced stages of pectoral fin development, being low at 8dpf and undetectable at 11dpf. a: anterior; p: posterior, pr: proximal; d: distal. Scale bar: 100 µm.

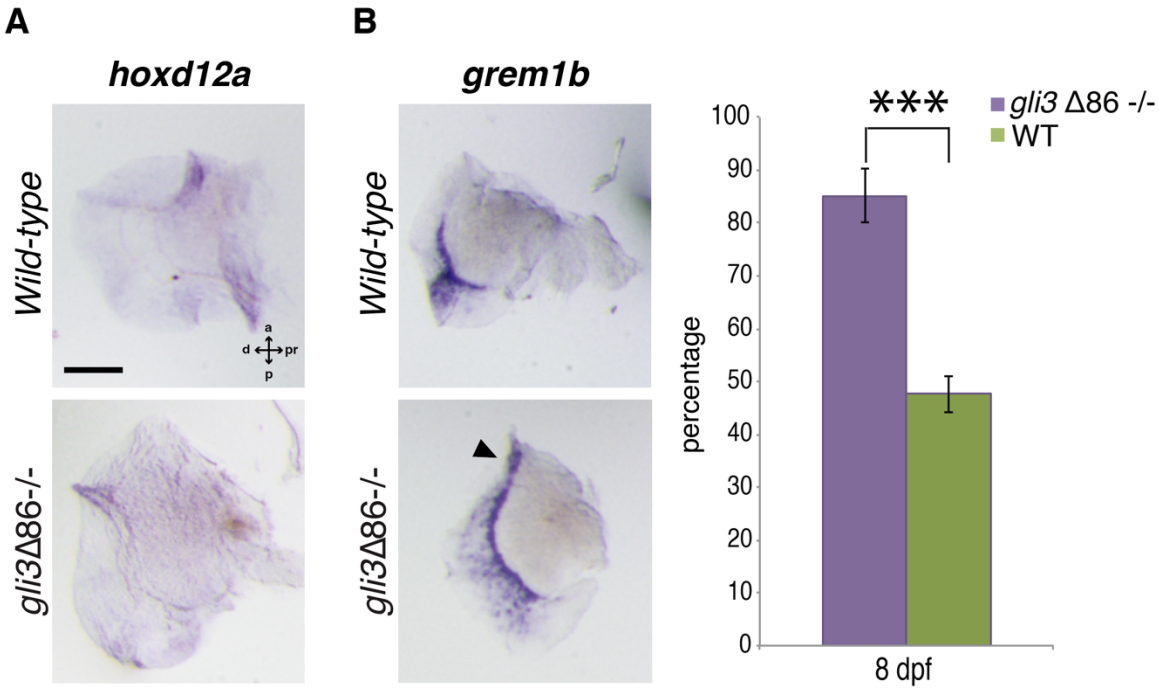

Fig. S3. Expression of *hoxd12a* and *grem1b* in wild-type and *gli3* mutant pectoral fin buds at 8 dpf.

(A) *hoxd12a* expression is strongly downregulated in the pectoral fins of wild-type and *gli3* mutant medaka embryos at 8dpf. (B) In 8dpf *gli3*-deficient pectoral fins, *grem1b* expression domain is anteriorly expanded along the distal rim of the endochondral disc in comparison to wild-type controls (arrowhead, left panels). This effect is independent of the size of the fin (right panel in B; proportion of the endochondral disc perimeter overlapping with *grem1b* expression; ***$P = 5.58 \times 10^{-8}$). a: anterior; p: posterior, pr: proximal; d: distal. Scale bar: 100 µm. n≥3 per marker and genotype.

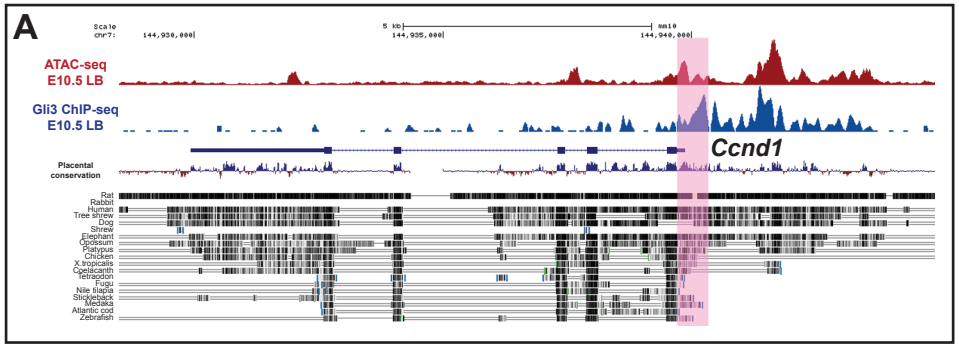
A
ATAC-seq
E10.5 LB
Gli3 ChIP-seq
E10.5 LB
Ccnd1
Placental
conservation

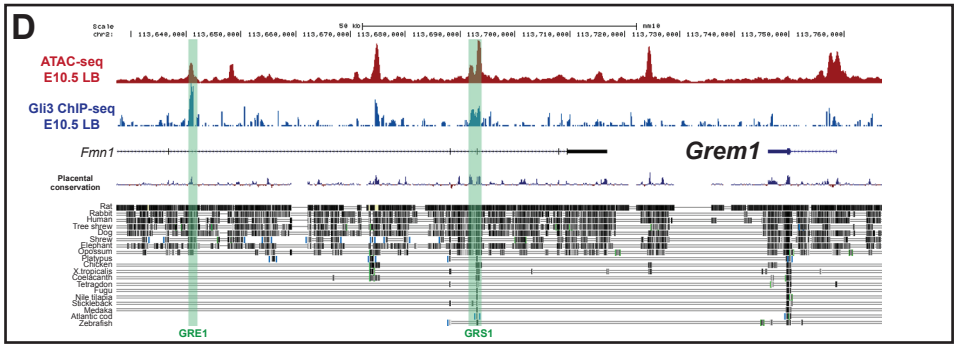
D
ATAC-seq
E10.5 LB
Gli3 ChIP-seq
E10.5 LB
Fmn1
Grem1
Placental
conservation
GRE1
GRS1

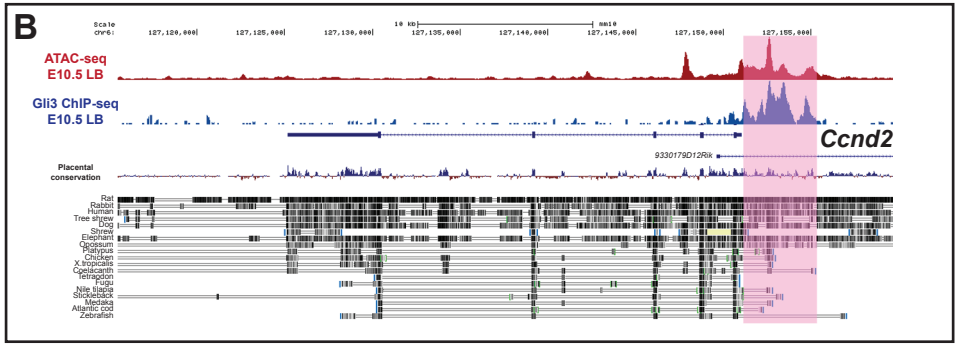
B
ATAC-seq
E10.5 LB
Gli3 ChIP-seq
E10.5 LB
Ccnd2
9330179D12Rik
Placental
conservation

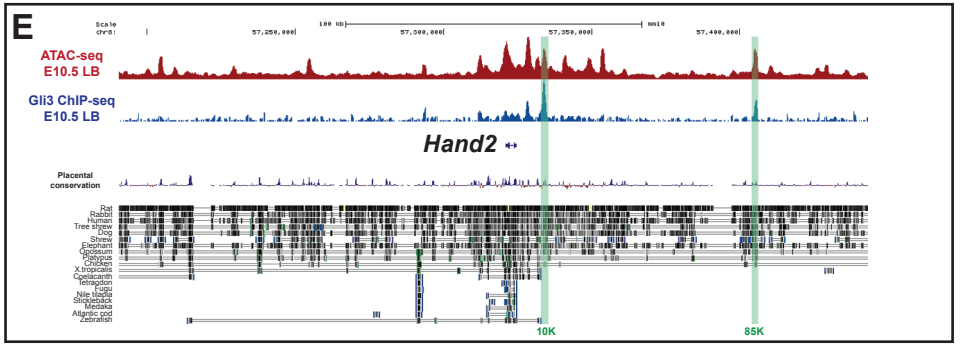
E
ATAC-seq
E10.5 LB
Gli3 ChIP-seq
E10.5 LB
Hand2
Placental
conservation
10K
85K

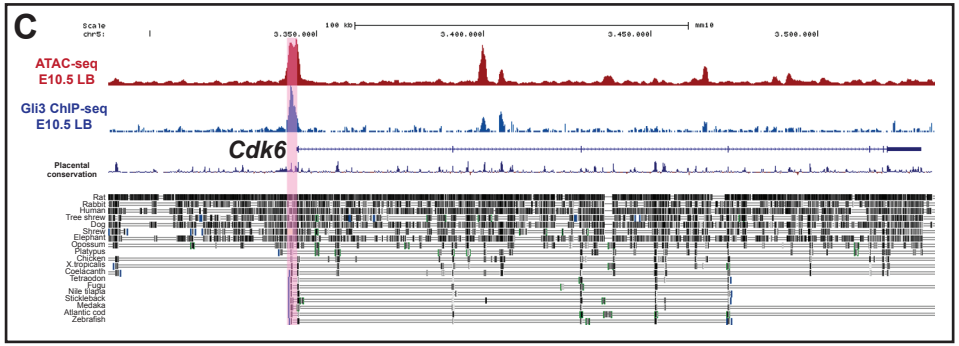
C
ATAC-seq
E10.5 LB
Gli3 ChIP-seq
E10.5 LB
Cdk6
Placental
conservation

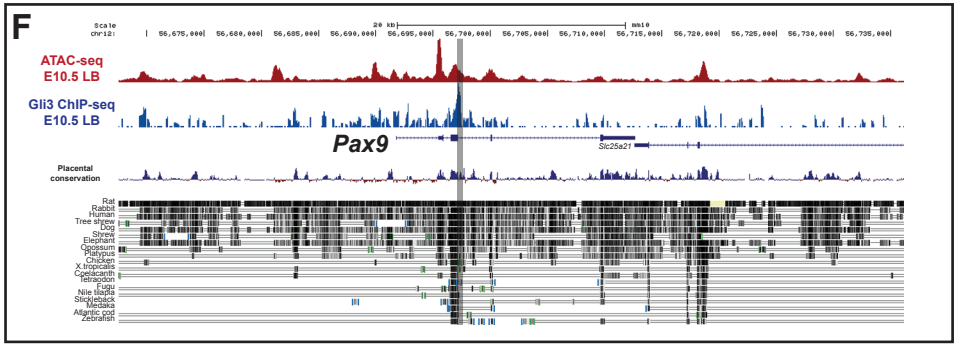
F
ATAC-seq
E10.5 LB
Gli3 ChIP-seq
E10.5 LB
Pax9
Slc25a27
Placental
conservation

Fig. S4. Regulatory landscapes of Gli3 target genes in mouse limb buds

(A-C) Genes encoding cell cycle modulators (A, *Ccnd1*; B, *Ccnd2* and C, *Cdk6*), are mainly regulated by Gli3 at the promoters through regions that are evolutionary conserved in fish genomes (highlighted in pink). Red tracks show ATAC-seq signal from E10.5 mouse limb buds (1). Blue tracks show Gli3 ChIP-seq data from E10.5 mouse embryonic limbs (2). (D-E) Genes involved in early limb patterning such as *Grem1* and *Hand2* are mainly regulated by Gli3 through distal CREs, most of them not conserved in fish genomes. *Hand2* regulatory regions (10K and 85K) were described in (3). Note that the *Grem1* GRS1 enhancer (4) is evolutionary conserved in teleosts, while the GRE1 regulatory element is not (3, 5). These previously identified Gli3-bound limb CREs are highlighted in green. (F) The *Pax9* genomic landscape in mouse limb buds contains a prominent Gli3-binding region within the gene body and overlapping an exon-intron boundary (grey shading). This region, of uncharacterized regulatory activity, is partially conserved in teleost genomes. LB: limb buds.

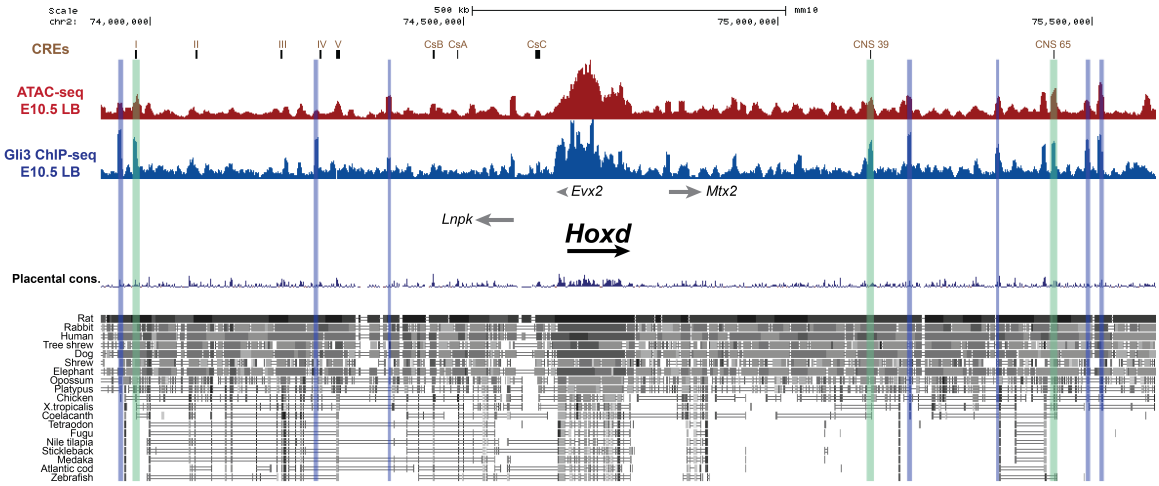

Fig. S5. The regulatory landscape of *Hoxd* genes in mouse limb buds

Profiles of accessible chromatin [ATAC-seq; red track (1)] and Gli3-occupancy [ChIP-seq; blue track (2)] within the mouse *Hoxd* regulatory landscapes in E10.5 limb buds. Of the main *Hoxd* cis-regulatory regions previously identified in mice [CREs: Islands I-V (6), CsA, CsB, CsC (7), CNS39 and CNS65 (8)], three are occupied by Gli3-containing complexes in mouse limb buds (Island I, CNS39 and CNS65; highlighted in green). Of these, only CNS65 is evolutionary conserved in teleosts and the orthologous fish sequences are able to drive reporter expression to the fin bud in transgenic zebrafish embryos (9). In addition, there are several uncharacterized Gli3-binding regions in the gene deserts [C-DOM and T-DOM TADs; (8)] flanking the *Hoxd* cluster, many of which cannot be found at the sequence level in teleost genomes (most prominent labelled in blue). There are also numerous Gli-associated regions within the *Hoxd* cluster itself, many of which overlap with transcribed regions, although the biological significance of these interactions is unknown. LB: limb buds.

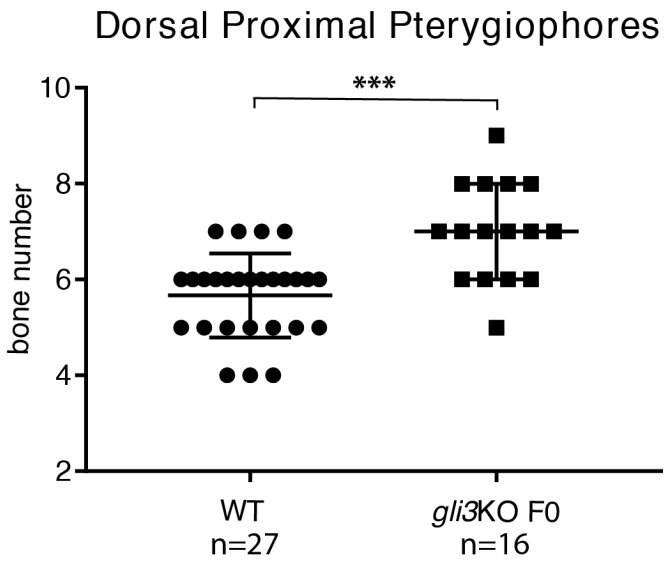

Fig. S6. g*li3* crispants show increased bone number in the adult dorsal fin.

Graph showing the number of proximal pterygiophore bones in the dorsal fin from WT and *gli3* F0 crispants. Each point in the graph represents bone number in a single fin. An unpaired t-test was used for the statistical analysis of bone number. ***$P = 5.33 \times 10^{-5}$ for the comparison between WT (mean = 5.666) and *gli3* crispants (mean=7). Microinjection of the *gli3* CRISPR mixture and skeletal staining were performed in three independent experiments.

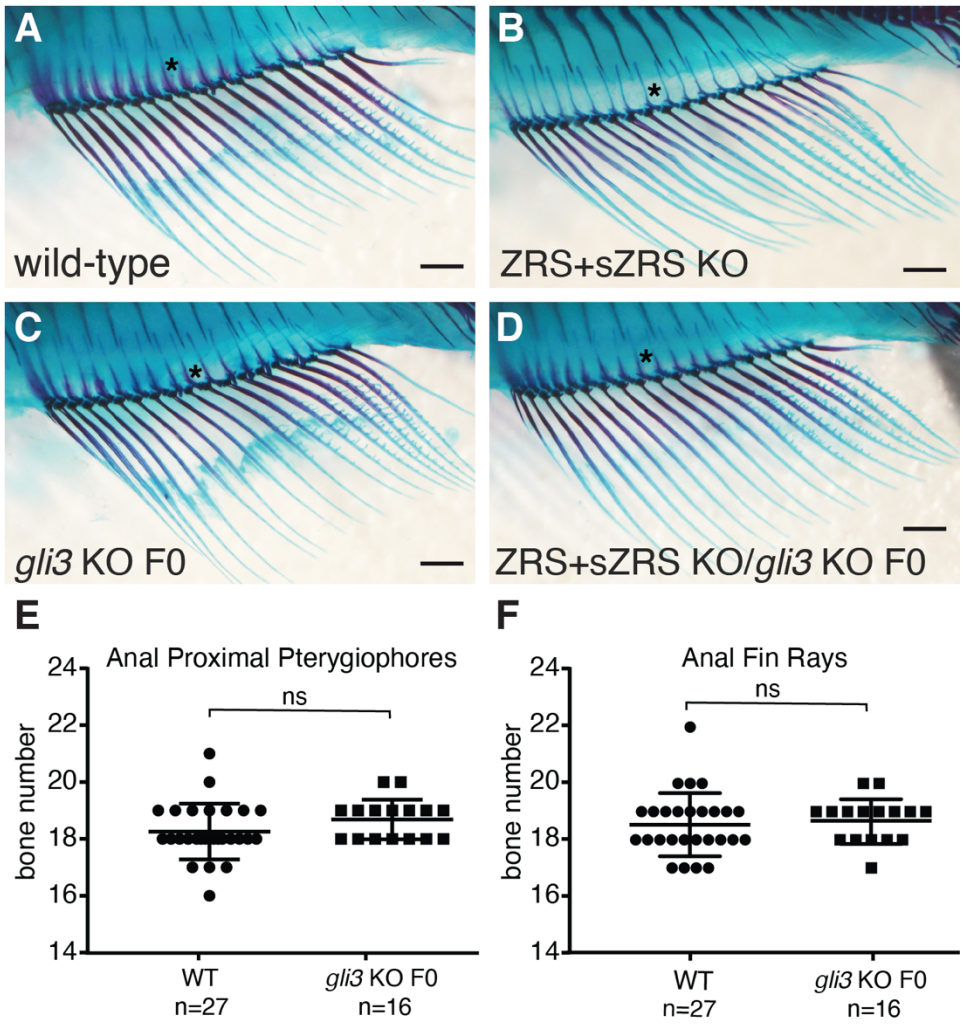

Fig S7. Anal fins are not affected in *gli3* and *ZRS+sZRS* single or compound mutants

(A-D) Skeletal staining showing adult (4m.o.) anal fins from WT (A), ZRS+sZRS KO (B), *gli3* KO F0 crispants (C) and compound *shh*/*gli3* KO F0 mutants (D). Scale bars 1mm. (E, F) No significant change in the number of anal proximal pterygiophores or fin rays was observed between WT and *gli3* F0 crispants. Each point in the graph represents the measurement of bone number in a single fin (n=27 WT, n=16 *gli3* KO F0). An unpaired t-test was used for the statistical analysis of anal proximal pterygiophore and fin ray bones. *P* = 0.1358 for the comparison between WT (mean = 18.26) and *gli3* crispant (mean = 18.69) anal proximal pterygiophores. *P* = 0.682 for the comparison between WT (mean = 18.56) and *gli3* crispant (mean = 18.69) anal fin rays. Note the delay in the ossification (asterisk) of the membranous blade that surrounds the stick of the proximal pterygiophore in both single and compound mutants when compared to wild-type fins. All pictures are lateral views with anterior to the left. Microinjection of the *gli3* CRISPR cocktail and bone staining procedures were performed in three independent experiments. ns: not significant.

Table S1. Primers sequences

a) Probe primers sequences

Name	Sequence 5'-3'	Vector	Enzyme for linearization	RNA polymerase	DNA source
Mdk_rprobe_hand2F	AGGCCACCACTACTCTTTGC	pGEM-T	PstI	T7	gDNA
Mdk_rprobe_hand2R	CTCCGTCTTCTTCAGGTCGG				
Mdk_rprobe_hoxd12a_Fw	GGGAATGGAACCCACATCC	Strataclone	BamHI	T3	gDNA
Mdk_rprobe_hoxd12a_Rv	CTTGCCCAAAAGTGGTCCT				
Mdk_rprobe_grem1F	TGGCTTGTTGTTCTCTCCCG	pGEM-T	NdeI	T7	gDNA
Mdk_rprobe_grem1R	CAAACACGCAGTCCAAGAGG				
Mdk_rprobe_pax9_Fw	TTCGGAGAGGTCAACCAGC	pGEM-T	PstI	T7	cDNA
Mdk_rprobe_pax9_Rv	GGTGGTTGTATGGTAACGCG				
Mdk_rprobe_gli3_Fw	CTAAAGGCCAAGTACGCAGC			SP6	gDNA
Mdk_rprobe_gli3_Rv_SP6	ATTTAGGTGACACTATAGAATACTGGGAATGAAGATACTGCACC				

b) Genotyping primers sequences

Name	Sequence 5'-3'
Mdk_genot_gli3_Fw	CGTGAGTTTCACAGCAACAATTA
Mdk_genot_gli3_Rv	CAGCCTCACTGATCAATTTCAG

c) qPCR primers sequences

Name	Sequence 5'-3'
Mdk_hand2_qPCR_Fw	GGACATCTTGGACAAAGACGG
Mdk_hand2_qPCR_Rv	GAGCTCAAGAGCCCAGACG
Mdk_hoxd12a_qPCR_Fw	GTGAACGGAACCAAGCAGG
Mdk_hoxd12a_qPCR_Rv	GGGCTTGGAGTAAGGCTTCC
Mdk_grem1_qPCR_Fw	GGGATGGTTTTCATCACTGG
Mdk_grem1_qPCR_Rv	CACATGTAACGCTTCCTGGC
Mdk_pax9_qPCR_Fw	GCCATGCACAGGATTTGG
Mdk_pax9_qPCR_Rv	GCTCACTGTGGGCGATCC
Mdk_ccnd1_qPCR_Fw	CCTCCTTGTCCTCTCAGAACC
Mdk_ccnd1_qPCR_Rv	ACAGGTCCACCTCTTCATCC
Mdk_ccnd2b_qPCR_Fw	CCTCCAAGCTGAAGGACTGC
Mdk_ccnd2b_qPCR_Rv	GATAACGGAGGCCATGTTCC
Mdk_cdk6_qPCR_Fw	ACGGAGGAAGAGGGAATGC
Mdk_cdk6_qPCR_Rv	CGAGCGTTAGTTTGGTTTCC
Mdk_gli3_qPCR_Fw	GCTTTGACCTGCAGATGATCC
Mdk_gli3_qPCR_Rv	GAGGGTAGGCGAAGTTCAGC
Mdk_ef1a_qPCR_Fw	AAACCCAGAAACACCGAAACAT
Mdk_ef1a_qPCR_Rv	CCTCCGCACTTGTAGATCAG

Supplementary References

1. V. Tissières *et al.*, Gene Regulatory and Expression Differences between Mouse and Pig Limb Buds Provide Insights into the Evolutionary Emergence of Artiodactyl Traits. *Cell Rep* **31**, 107490 (2020).
2. R. K. Lex *et al.*, GLI transcriptional repression regulates tissue-specific enhancer activity in response to Hedgehog signaling. *Elife* **9** (2020).
3. S. A. Vokes, H. Ji, W. H. Wong, A. P. McMahon, A genome-scale analysis of the cis-regulatory circuitry underlying sonic hedgehog-mediated patterning of the mammalian limb. *Genes Dev* **22**, 2651-2663 (2008).
4. A. Zuniga *et al.*, Conserved cis-regulatory regions in a large genomic landscape control SHH and BMP-regulated Gremlin1 expression in mouse limb buds. *BMC Dev Biol* **12**, 23 (2012).
5. Q. Li *et al.*, A Gli silencer is required for robust repression of gremlin in the vertebrate limb bud. *Development* **141**, 1906-1914 (2014).
6. T. Montavon *et al.*, A regulatory archipelago controls Hox genes transcription in digits. *Cell* **147**, 1132-1145 (2011).
7. F. Gonzalez, D. Duboule, F. Spitz, Transgenic analysis of Hoxd gene regulation during digit development. *Dev Biol* **306**, 847-859 (2007).
8. G. Andrey *et al.*, A switch between topological domains underlies HoxD genes collinearity in mouse limbs. *Science* **340**, 1234167 (2013).
9. I. Braasch *et al.*, The spotted gar genome illuminates vertebrate evolution and facilitates human-teleost comparisons. *Nat Genet* **48**, 427-437 (2016).